Manipulation of Suspended Single Cells by Microfluidics and Optical Tweezers

Nathalie Nève,[1] Sean S. Kohles,[1,2] Shelley R. Winn,[3,4] and Derek C. Tretheway[1]

[1]Department of Mechanical & Materials Engineering, Portland State University, P.O. Box 751, Portland, OR 97201, USA; [2]Department of Surgery, Oregon Health & Science University, Portland, OR 97239, USA; [3]Department of Restorative Dentistry, Oregon Health & Science University, Portland, OR 97239, USA; and [4]Department of Molecular & Medical Genetics, Oregon Health & Science University, Portland, OR 97239, USA

Abstract—Chondrocytes and osteoblasts experience multiple stresses *in vivo*. The optimum mechanical conditions for cell health are not fully understood. This paper describes the optical and microfluidic mechanical manipulation of single suspended cells enabled by the μPIVOT, an integrated micron resolution particle image velocimeter (μPIV) and dual optical tweezers instrument (OT). In this study, we examine the viability and trap stiffness of cartilage cells, identify the maximum fluid-induced stresses possible in uniform and extensional flows, and compare the deformation characteristics of bone and muscle cells. These results indicate cell photodamage of chondrocytes is negligible for at least 20 min for laser powers below 30 mW, a dead cell presents less resistance to internal organelle rearrangement and deforms globally more than a viable cell, the maximum fluid-induced shear stresses are limited to ~15 mPa for uniform flows but may exceed 1 Pa for extensional flows, and osteoblasts show no deformation for shear stresses up to 250 mPa while myoblasts are more easily deformed and exhibit a modulated response to increasing stress. This suggests that global and/or local stresses can be applied to single cells without physical contact. Coupled with microfluidic sensors, these manipulations may provide unique methods to explore single cell biomechanics.

Keywords—Chondrocytes, Osteoblasts, Applied fluid and mechanical stresses, Cell biomechanics, Cell deformation.

INTRODUCTION

In the United States, osteoarthritis affects over twenty million people, a number predicted to double in the next 20 years. Biomechanical factors such as excessive repetitive loading may negatively influence cartilage and bone cell behavior leading to pathological matrix synthesis and increased tissue degradation.

Healthy chondrocytes and osteoblasts experience multiple stress states resulting from hydrostatic, hydrodynamic, compressive, tensile, and shear forces that maintain the phenotype and production of new tissue. However, optimum mechanical conditions are not completely known. Moreover, the process of mechanotransduction, which transforms the mechanical environment experienced by cells into a biomolecular response, has not been fully characterized at the single cell level.

The promise and contribution of biomechanics is to advantageously control cell function in the treatment of disease or in regenerative medicine.[28] Exploring biomechanics at the cellular level is now becoming feasible thanks to the advances in technology. A number of techniques exist to characterize cell membrane and cytoplasm mechanics. Micropipette aspiration applies a negative pressure to the cell for localized membrane stretching with results reported for red and white blood cells,[6,12,21,61] endothelial cells,[60] as well as chondrocytes.[27] Cytoindentation incorporates a probe (such as a 2 μm diameter glass microfiber) that compressively loads a cell adhered to a surface.[14,52,54] Atomic Force Microscopy (AFM) manipulates a cantilevered probe (tip radius ranging from a few nanometers to a few micrometers) for tension or compression loading.[20,55,59] A slightly larger version of the AFM technique facilitates microscale indentation of an entire cell.[32,39] Microplates, either rigid or flexible, can apply a range of mechanical stresses to an entire cell including tension or compression.[66] Other than the micropipette technique, most evaluations of single cells or groups of cells require surface attachments to provide a reaction force. These surface adhesions constrain the cell and may or may not involve additional cytoskeletal manipulation such as the binding of integrins to ligands. This compounds the cellular mechanical response.

Address correspondence to Derek C. Tretheway, Department of Mechanical & Materials Engineering, Portland State University, P.O. Box 751, Portland, OR 97201, USA. Electronic mail: derekt@cecs.pdx.edu

Contact-free cell deformation applying innovative techniques has been explored to a lesser extent. One of the oldest techniques, the rheoscope[62] examined red blood cells by measuring blood viscosity as a function of cell deformation and cell aggregation. Later, using the rheoscope as well as an ektacytometer, Bull *et al.*[6] studied the elliptocytic red cells deformability under different shear stresses. The appearance of optical tweezers and derived technology in the late 1980s opened the door to new testing of cells without physical contact. In the optical channel,[29] hydrodynamic stresses elongated red blood cells passing through a focused beam. In the optical stretcher,[18] a cell is held and stretched optically. Because the beam is not focused, higher powers can be applied to manipulate the cell without damaging it.

In an effort to characterize multiaxial and multimodal cellular biomechanics, Nève *et al.*[49] developed the integrated micron-resolution particle image velocimetry (μPIV) and dual optical tweezers (OT) instrument, the μPIVOT. μPIV measures local fluid movement by tracking fluorescent nanoscopic seed particles excited with dual pulsed 532 nm lasers. Dual OT allow for the capture, suspension, and direct manipulation of isolated single cells by optical gradient forces resulting from a focused infrared laser. The combination of these two techniques provides a unique platform for controlling and monitoring cellular biomechanics (stress and strain) as a precursor to deciphering mechanobiology. As an enhancement to the μPIVOT, microfluidics provide additional control of the local fluidic microenvironment including applied shear and normal stresses.

This paper provides a brief overview of the μPIVOT, describes its integration with microfluidics, and presents results of this new approach for three-dimensional (3D) mechanical manipulation of single cells. The study examines the viability and trap stiffness of chondroblasts, identifies the maximum fluid induced stresses possible in representative uniform and extensional flows, and compares the deformation characteristics of osteoblasts and myoblasts. The overall objective of this work is to outline a method to explore individual cellular biomechanics.

THE μPIVOT

Figure 1 shows the schematic of the μPIVOT, a system integrating two laser-based techniques, micron-resolution particle image velocimetry (μPIV) and optical tweezers (OT),[49] within a Nikon TE2000 inverted microscope with a $60\times$, N.A. 1.45, oil immersion Plan Apo TIRF objective lens. The instrument allows non-contact OT manipulation of single cells in microfluidic environments, the potential for full characterization of applied hydrodynamic stresses with μPIV, and measurement of resulting cellular strains.

μPIV

Micron-resolution particle image velocimetry is a two-dimensional (2D) full field flow velocity measurement technique capable of resolving velocity fields to within 436 nm of a microchannel wall.[71] Details of the μPIV technique can be found in Nguyen and Wereley.[50] Velocity measurements are obtained by seeding the flow domain with fluorescent nanoparticles, volume illuminating the region of interest with pulses from two frequency doubled Nd:YAG lasers at the nanoparticle excitation wavelength, and imaging the emitted light by selectively removing the excitation wavelength with an epi-fluorescent filter. The lasers are synchronized with the charge-coupled device (CCD) camera such that the camera captures the emitted particle light from each laser pulse on consecutive image frames. With this configuration the separation time between image pairs (as short as 200 ns) is independent of the camera framing rate. Thus, the time between image pairs can be optimized for given velocities and the desired spatial resolution. The resulting image pairs are cross-correlated and ensemble averaged (for steady or phase locked, periodic flows) to increase the nanoparticle signal to noise ratio.[45] Note, only particles within the focal plane of the objective lens contribute significantly to the correlation, effectively confining the velocity measurement to a single plane.

OT

Optical tweezers or optical trapping is capable of suspending and manipulating micron-sized objects with nanometer position detection and applied forces on the order of pico-Newtons.[1,37] In brief, an optical trap is produced by passing a laser beam through a high numerical objective lens and focusing it to its diffraction-limited spot. For particles larger in dimension than the wavelength of the trapping laser (like a biological cell), the mechanism for particle trapping is described by a ray optics approach that indicates that individual rays of light are refracted as they pass through the trapped object. This change in direction and the associated momentum, imparts an equal and opposite force on the object. Without additional imposed forces, an object is trapped at the focal point. Actual trap behaviors such as trap stiffness are calibrated experimentally since the trapping force depends on the trapped particle material (here a biological cell), laser power and intensity profile, particle shape,
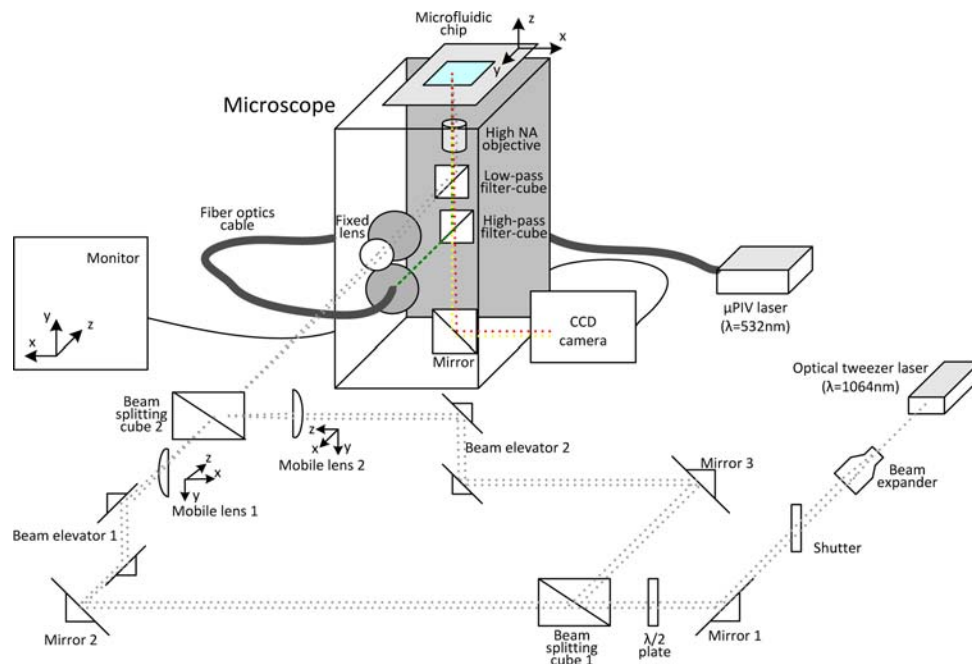
FIGURE 1. Schematic of the µPIVOT device and the current optical arrangement. The OT laser goes through different optical components including beam splitting cubes to allow the existence of two lasers of opposite polarization. The position of their focus point can be controlled independently using two mobile lenses that translate in any direction with automated control (0.1 µm resolution). Both traps can operate simultaneously or individually using shutters placed in the laser beams paths. Both of the OT lasers reunite through a second beam splitting cube before entering the microscope through an optical port. The µPIV lasers enter through a second port via an optical cable.

particle size, and fluid media. The damage on the cell due to the trapping laser has not been fully characterized but it is known to heat the cell depending on the applied laser power and wavelength.[1,2,35] For the µPIVOT, a 1064 nm wavelength laser was chosen to minimize laser absorbance by the cells.[48]

MATERIALS AND METHODS

Cell Culture

In collaboration with the Oregon Health & Science University (OHSU), primary cultures of chondrogenic and osteogenic tissues were generated from rat long bones. We followed the procedures and protocols for bone and cartilage cell isolation described in Jones.[26] Further information on isolation, proliferation, and differentiation of osteoblastic cells can be found in Declercq *et al.*[9] The muscle cells used in the present studies were the mouse derived myoblast C2C12 cell line obtained from ATCC (CRL-1772; Manassas, VA). Cells were cultured in tissue culture flasks using α-MEM (Cellgro, Herndon, VA) supplemented with 10% fetal bovine serum (GIBCO, Gaithersburg, MD), 2% glutamine, 1–2% penicillin–streptomycin (Cellgro), and 2% 1 M HEPES under standard culture conditions[24] (37 °C, 5% CO_2, pH 7). Cells were cultured up to 4 passages for all experiments. P0 (= passage 0) was the batch of cells directly harvested from the cartilage tissue and consisted mainly of chondrocytes (rounded cells) and chondroblasts (attached). Osteogenic cultures exhibited firmly attached osteoblasts with a typical epithelial morphology. Myoblasts were firmly attached elongated cells that retained the ability to form myotubes when exposed to tissue culture medium with reduced serum content (2%). Cells from older than 4 passages were not used due to their tendency to de-differentiate. On the day of experimentation, cells were detached from the flask surface with 0.05% trypsin–EDTA (Ethylenediamine tetraacetic acid, GIBCO). Harvested cells were diluted (10000 cells/mL) in a solution containing 50 mL of artificial cerebrospinal fluid, 1 mL of HypoThermosol FRS (BioLife Solutions, Bothell, WA), and one micromolar of EDTA to avoid clustering. Cells were examined at room temperature for all experiments (~20.5 °C). The flow media consisted of a physiological buffer (127 mM NaCl, 5 mM KCl, 2 mM $MgCl_2$, 0.5 mM Na_2HPO_4, 2 mM $CaCl_2$, 5 mM $NaHCO_3$, 10 mM glucose, 10 mM HEPES, 0.1% BSA adjusted to pH 7.4).

Cell Reservoirs and Microfluidic Device Fabrication

To test cells under various mechanical stimuli such as local or global stresses in static or dynamic environments, multiple microfluidic devices were created. To study cell responses to local OT-induced stresses and global hydrodynamic stresses of uniform flows, a simple rectangular reservoir was constructed. These simple reservoirs were modified slightly to investigate the action of hydrostatic pressure on the cells by adding variable height input and exit ports. To study cells subjected to more complex flows (such as an extensional flow), microfluidic chips were designed and fabricated. In each device, an isolated cell is suspended by the optical tweezers without attachment to any surface or mechanical restraint.

Cell Reservoirs

Figure 2a provides an image of a simple cell reservoir defined by four walls of double-face tape (foam mounting tape of approximately 1 mm thick) attached to a coverslip. The reservoir is filled with a solution of diluted cells (10000 cells/mL) and enclosed by a second coverslip. The reservoir was then placed on an automated stage (H117 ProScan^TM II stage, Prior Scientific, Rockland, MA) that was either stationary for static experiments or moving at constant velocity to generate a uniform flow field around a suspended cell held at a fixed position.

To investigate the effects of hydrostatic pressure, the reservoir was modified to include variable height input and output ports which consisted of Tygon tubing (Fisher Scientific, Pittsburgh, PA) sealed to the reservoir with Epoxy. The input tubing was connected to an open syringe (no plunger) attached to a vertical micrometer for fluid height displacement (Fig. 2b).
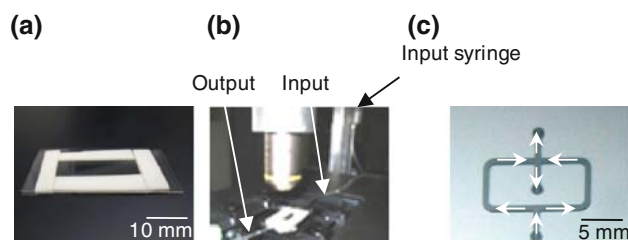
Microfluidic Chip

Figure 2c shows the microfluidic chip, silicone mold of a cross-junction channel. This geometry creates an extensional flow environment with a stagnation point at the cross-junction geometric center. A cell may be positioned at this point and subjected to hydrodynamic stresses without a net drag force. Two iterations of the cross-junction design were initially fabricated with an elimination of the cell reservoir design in the current version, as it was observed that static cells tended to cluster and stick to the walls of the reservoir after approximately 20 min. The chip was fabricated using a standard soft lithography approach with polydimethylsiloxane (PDMS) (Sylgard 184, Dow Corning, Midland, MI) as the soft peeled material. The PDMS chip was bonded to a cover slip, after having punched 20 gage holes (~0.9 mm) for microport access. A gravity driven flow was generated by simply attaching input and output open syringes placed at different heights. The output syringe height was held constant while the input syringe height was adjusted in order to vary the flow rate. Velocities up to 750 μm/s were produced by fluid heads of 2.5 cm. The syringes were connected to the microfluidic chip via Tygon tubing (Fisher Scientific, Pittsburg, PA) attached to metal pins (23 gage, 0.025″ OD × 0.017″ ID, Stainless steel type 304, New England Small Tubes Corp., Litchfield, NH) that were directly inserted into each of the entry/exit ports of the microchannel. The resulting microfluidic chip arrangement allowed for a controllable, constant, and steady flow.

Experimental Protocols

Static Environment: OT-Induced Stress and Hydrostatic-Induced Stress

This study has explored local and global stresses applied to cells in a static environment. Local stresses were also applied directly using the dual OT. Global stresses were induced hydrostatically.

For local stress experiments, a low concentration of 10000 cells/mL was placed in the rectangular reservoir. A cell was trapped with the dual trapping beams (an equally split laser) and positioned a few microns away from the coverslip surface. A range of laser powers (30 mW up to 1 W at the sample) was applied to the cells while their viability was monitored through Trypan blue absorption (1:1 volume ratio) added to the culture media. For stretching of the cell with two optical traps, one trap remains fixed while the second one is slowly directed away from the center of the cell. Trap movement is controlled by positioning lenses located on automated vertical and linear stages (MVN80 and UMR8.25, Newport). The stage

FIGURE 2. Microfluidic chip design (a) Cell reservoir used for static experiments and uniform flow experiments (30 mm × 10 mm). (b) Cell reservoir used for hydrostatic experiments. The input is set at different heights while the output is closed. (c) Silicone mold of the cross-junction channel. The channels are 50 μm deep × 500 μm wide. White arrows show the directions of the flow.

translation range of 25 mm × 25 mm × 12.5 mm provided trap movements in excess of the field of view.

Due to its ease of application and the homogeneous stress environment, hydrostatic pressure was applied to the cell for global static stress measurements. In these experiments, a low concentration of cells (10000 cells/mL) solution was placed in the input syringe. The output tubing was opened to air and maintained at the reservoir height while the input syringe was slightly raised to fill the reservoir. After elimination of all air bubbles in the system, the output tubing was clamped to halt the flow and a static environment was obtained. A cell was then trapped a few microns away from the coverslip at the minimum power (approximately 30 mW at the sample) to position and maintain the cell in focus. Hydrostatic pressure was varied by adjusting the input syringe height relative to the reservoir. A maximum syringe height of 10 cm was applied.

Dynamic Environment: Uniform and Extensional Flows

To apply hydrodynamic forces, a simple uniform flow was generated by trapping a cell and moving the automated stage at a constant velocity. Cells were trapped at the minimum laser power (30 mW at the sample) to minimize potential radiation damage to the cell.

Under uniform flow conditions, the cell undergoes two main forces: the applied drag force (F_{drag}), due to hydrodynamic stresses on the cell and the reacting trap force (F_{trap}). For statically stable trapping, these forces are equal in amplitude and opposite in direction. From the experiments, two parameters can be determined: (1) the cell deformation D_{12}; and (2) the trap stiffness k. D_{12}, the Taylor deformation parameter,[5] is computed by measuring the major and minor axes of the cell (L and B respectively), such that $D_{12} = (L - B)/(L + B)$. The axes are measured using the NIH open software ImageJ. An ellipse aligned with the flow direction was superimposed on the cell image to fit the general outline of the cell boundary. The axes of the ellipse are recorded and taken as the minor and major axes. If the cell is smooth sub-pixel ($< 0.125\ \mu$m) accuracy in the axes length or position can be achieved. However, since the cell surface may be rough, the ellipse axis resolution with this method is ± 2 pixels ($0.250\ \mu$m). The trap stiffness, k, is calculated by equating the drag force to the trap force, $F_{drag} = F_{trap}$. F_{trap} is equal to $k \cdot \Delta x$ for small displacements (the linear regime) where Δx is the difference between the cell position (geometric center) when trapped without flow and trapped with flow. Note, we only calculate k for the linear regime where the displacement as a function of drag force has a linear fit of $R^2 > 0.9$. Since cell deformation is sufficiently small (cell protrusions

are negligible as well) in this study, we can assume the cell is spherical thus $F_{drag} = F_{Stokes}/C$, where $F_{Stokes} = 6\pi\mu a v_\infty$ (Stokes drag), C is a correction factor which accounts for particle–wall effects associated with the presence of the bottom coverslip, μ is the fluid dynamic viscosity, v_∞ is the fluid velocity away from the sphere, and a is the radius of the cell. The correction factor,[19] C, is equal to $1 - (9/16)(a/l) + (1/8)(a/l)^3 - (45/256)(a/l)^4 - (1/16)(a/l)^5$ where l is the distance of the cell from the bottom coverslip. The distance, l, was determined by calculating the difference between the objective lens position (precision ~0.1 μm) when a cell was trapped during the experiment and the objective lens position at the coverslip (determined by both reflection of the optical trap at the coverslip and by focusing on a cell resting at the coverslip and subtracting the cell radius from the objective lens position). A factor of 0.878 is applied to account for the focal shift due to the index of refraction mismatch between the culture media ($n_f = 1.33$) and the coverslip/immersion oil ($n_g = 1.515$). The top coverslip does not need to be considered in the calculations. Its effect is negligible ($C > 0.99$) as it is approximately 1 mm away from the bottom coverslip and thus several hundreds of microns away from the cell. Note, in the above calculations, the effects of possible spherical aberrations due to the index of refraction mismatch between the culture media ($n_f = 1.33$) and the coverslip/immersion oil ($n_g = 1.515$) on trap stiffness measurements were not taken into consideration because the effect is inconsistent as demonstrated in the studies by Fallman and Axner[13] and Im et al.[23] Regardless, to minimize errors that could be introduced due to the difference of the trap behavior with sample depth and optical aberrations, all cell and calibration experiments in uniform flow were conducted at the same distance from the coverslip.

A limiting factor in the uniform flow experiments is the maximum hydrodynamic stress that can be applied to a cell. As the velocity increases, so do hydrodynamic stresses and fluid drag. To overcome this increase in drag and maintain a stable trapped cell, the trap power must be increased. This may lead to potential damage of the cell. In order to increase the hydrodynamic stress applied to the cell and alleviate potential radiation damage, fluid flows which generate no net drag are required.

Planar extensional flow has been used extensively in the study of drop deformation and breakup.[4,5,70] This symmetric flow contains a stagnation point. A symmetric particle centered at the stagnation point experiences no net drag. In this work we created a pseudo-planar extensional flow in a microfluidic cross junction. Microfluidic cross junctions have mainly been used for droplet generation[74,75] and combining fluid

flows. The flow arrangement for droplet generation consists of three inlets (usually, the two opposite inlets introducing oil, and the third inlet being an immiscible fluid from which the droplets are formed), and one outlet, where droplet formation occurs. However, in our experiments we apply a cross-junction to generate fluid compression along the two opposing fluid inlets and fluid extension along the fluid outlets. The components of the fluid velocity (v_x, v_y) in the directions of the extensional and compressional axes vary linearly with position such that $v_x = \gamma \cdot x$ and $v_y = \gamma \cdot y$, where γ is the shear strain rate, x is the distance from the stagnation point along the extensional axis and y is the distance from the stagnation point along the compressional axis. Figure 3 shows μPIV velocity data for fluid flow in a cross junction. When a cell is held stationary at the stagnation point, it experiences compressive and tensile stresses whose magnitude depends on the flow rate.[33] Integration of these stresses around the cell yields no net drag force regardless of flow rate.

To apply an extensional flow on a cell, the cross-junction microfluidic chip is first primed by inserting a low concentration of cells (10000 cells/mL) through the upstream tubing. The low cell concentration is high enough to locate and trap a cell but sufficiently dilute to minimize flow disturbances from the remaining untrapped cells and to maintain Newtonian fluid behavior. A single cell is chosen and followed by moving the microscope translation stage at the same velocity and direction as the flow until it is close to the stagnation point. The cell is then trapped by a single OT and placed at mid-width and mid-height of the channel in order to avoid any cell rotation due to the
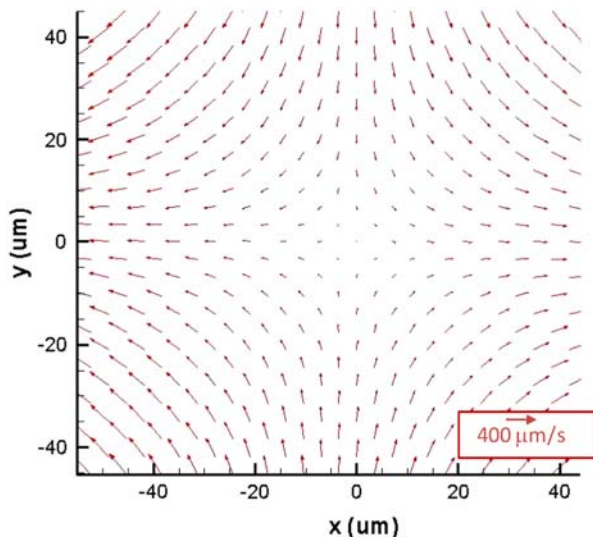

FIGURE 3. The undisturbed velocity field of a cross-junction flow near the stagnation point. Velocities are measured with μPIV.

velocity gradients across the channel. The hydrodynamic pressure and fluid flow is finally increased by slowly and continuously raising the input syringe. The use of gravity driven flow provides a very smooth flow with no oscillation and no perturbations on the stagnation point location. Variations of the hydrostatic head provide two effects: variation of hydrostatic pressure and flow rate. CCD images of cells are recorded at known input and output syringe heights to monitor cell behavior and determine cell deformation. All the experiments were performed with a 1064 nm Nd:YVO$_4$ trapping laser, at low powers (30 mW) and for a short period of time (less than 4 min).

RESULTS AND DISCUSSION

Coupled with microfluidics, the μPIVOT provides a unique ability to subject the same individual cell to a wide range of static and dynamic mechanical stress conditions. An individual cell can be exposed to a sequence of mechanical stresses such as OT extension or compression, hydrostatic pressure, or fluid induced shear or extension. These stress conditions can be applied sequentially or simultaneously. With the μPIVOT instrument combined with microfluidics, an entire mechanical stress sequence can be applied without changing equipment, altering the culture media, or examining a completely new cell and can be implemented quickly with minimal cell deterioration due to culture time. Moreover, with the imaging capabilities of μPIV, local velocity fields may be calculated and cell morphology determined. From the velocity field, the stresses applied to the cell at any location (within the focal plane) along the cell membrane/fluid interface may be computed. The following preliminary results show the capabilities of the instrumentation on biological cells, as well as the use of μPIV with polystyrene microspheres.

Optical Trap-Induced Stress

Cell Viability During Optical Tweezing

To our knowledge, no viability tests have been performed specifically for bone and cartilage cells subjected to optical tweezers. Although not our primary focus, quantifying cell viability is necessary to assure cell health during experiments. Numerous studies have investigated cell health and viability under optical traps through assays such as cell proliferation, cell mobility, and DNA structure. These studies show that the cell viability depends on the trapping wavelength, the power density, energy density, and the exposure duration. Liang *et al.*[40] showed no adverse effect on hamster ovary cell cloning efficiency when

trapped with a 1064 nm laser at 175 mW for less than 3 min. Under similar conditions, Neuman *et al.*[48] examined bacteria mobility (*Escherichia coli*) and observed limited photodamage due to optical traps. Liu *et al.*[43] investigated the effect of 1064 nm laser on DNA structure, cell viability and pH levels of hamster ovary cells as well as human sperm cells: no effect was observed when the laser power was under 300 mW for less than 2 min.

Two effects of laser trapping on biological specimens are laser-induced heating and photodamage. With water being the main component of biological cells (approximately 70%), laser induced heating is relatively mild for laser wavelengths of 200–1100 nm, where water absorption is small. Liu *et al.*[42] showed that for a laser operating at 1064 nm laser-induced heating is 1.15 °C for every 100 mW of laser power entering a hamster ovarian cell trapped in a stationary fluid. Thus, for our experiments where the laser power is 30 mW and a cell is trapped in a moving fluid (more efficient heat transfer), we would expect a cell temperature increase of less than 0.38 °C, if we assume the relationship between temperature increase and laser power follows Liu *et al.*[42] and is linear. This level of laser-induced heating was assumed to have minimal influence on cell health.

To assess any optical damage of trapped cells, cell morphology was monitored and compared to non-trapped cells. In general, healthy live cells have distinct edges, are smaller in volume, and appear smoother, denser and more contained than dead cells. To determine viability, Trypan Blue, known to enter the intracellular space due to an increase in membrane porosity of dead or dying cells,[65] was introduced at a 1:1 ratio. A morphology and viability benchmark was determined by trapping cells at maximum power (~1 W at sample). Figure 4 provides the evolution of Trypan Blue uptake and net cell volume increase under these conditions. The results show a slight (visually insignificant) net cell volume increase and Trypan Blue uptake (decrease in intensity) during the first 20 s of applied laser power followed by a rapid increase (visually apparent) in net cell volume and Trypan Blue uptake. This indicates a change in the permeability of the cell membrane, a sign of cell damage. Within 35 s, Trypan Blue was clearly visible in the cell (Fig. 4). During cell biomechanics experiments, we monitored cell morphology and Trypan Blue uptake (if added). At typical laser powers (30 mW measured at the sample) no morphological change was observed over the experimental timeframe, an average of 20 min.

Cell Manipulation by Two Optical Traps

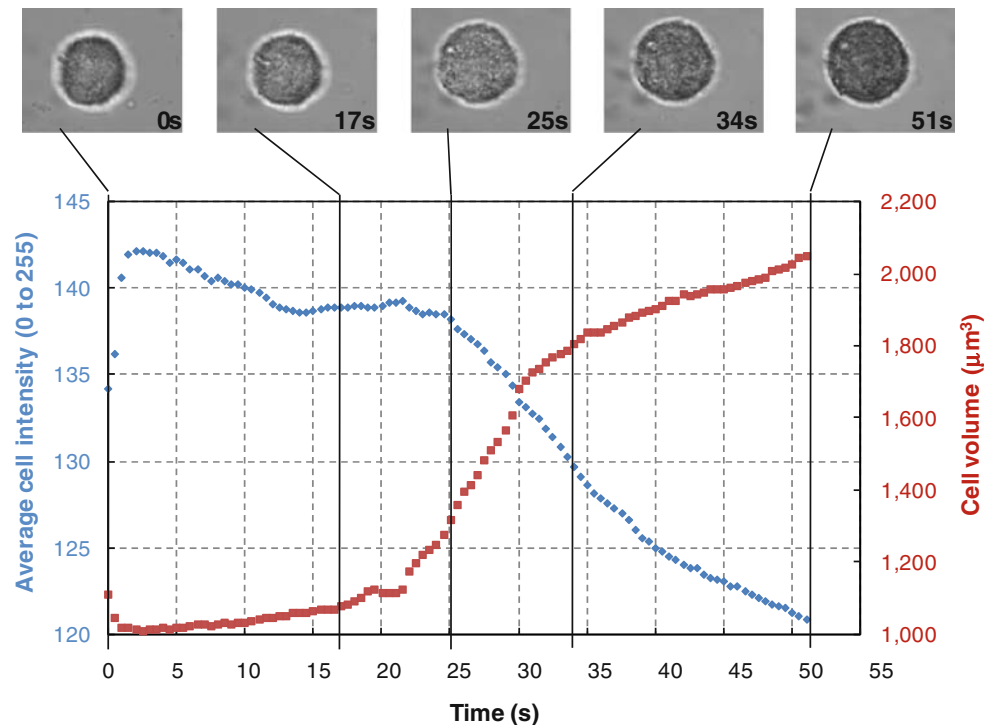The most common method to stretch cells or smaller entities such as macromolecules is to trap attached

FIGURE 4. Representation of pixel intensity and volume changes of a 15.5 μm diameter chondroblast under a high powered optical trap (~1 W at sample), with representative pictures at indicated time points. The cell membrane becomes permeable after ~20 s and the volume increases suddenly. After 35 s, the uptake of Trypan blue by the cell becomes visible.

beads arranged as "handles".[46,63] The primary advantage of this technique is the ability to induce higher cell deformation without inflicting increased optical damage to the cell (the laser energy is focused on the trapped beads). As the presence or absence of focal adhesions of a cell to a surface is known to alter the cytoskeleton, a potential disadvantage of this technique is the method of attachment of the bead to the cell surface. Since actin stress fibers are anchored at focal points and spread through the intracellular arrangement, cell-surface attachments modify a cell's shape and motility.

In order to gain insight on the elastic properties of the cell without the effects of physical attachment, we direct two optical traps directly into the cell and focus on intracellular organelles. Liao *et al.*,[41] used this method to stretch a trapped red blood cell by jumping the focal point of an optical tweezers between two locations at 100 Hz. Figure 5 shows the physical response of a "dead" and live chondroblast subjected to opposite movement of the optical traps. The sequence of Figs. 5a–5c shows trapping of an organelle inside a cell we believe to be dead. Morphologically, the cell is larger, the internal structures are less dense, and the edge is less distinct. This morphology is consistent with other cells tested that showed a rapid uptake of Trypan Blue when added to solution. Figure 5c shows that the organelle can be pulled out of the cell with limited resistance. This organelle could be a number of cell sub-units approximately 1 μm in size such as a small mitochondria, a lysosome, a vacuole, or a vesicle. Wei *et al.* have trapped submicron organelles of epithelial cells.[72] In Fig. 5b, the cell deformation is

at a maximum with a Taylor deformation parameter (D_{12} defined previously) of 0.15. On the contrary, Fig. 5e shows that the viable cell is slightly stretched at its maximum deformation of 0.05. Any attempt to induce further deformation by additional movement of the OT, resulted in the cell disconnecting from the dual traps and repositioning around a single trap. This suggests that one can probe the viability of a cell by monitoring the deformation characteristics of the cell and/or the rearrangement of the cell's internal structure. It is interesting to note that while an alive or dead cell stretches throughout its volume, a local deformation (a small protrusion) around the vicinity of the laser focus is observed (Fig. 5e).

Recent AFM studies have shown that the stiffness of bacteria can either increase or decrease after death. Francius *et al.*[16] showed a decrease in cell stiffness after the digestion of the cell wall by Lysostaphin. On the contrary, Cerf *et al.*[7] showed an increase in cell stiffness after deadly heating of the entire cell, which is hypothesized to collapse the lipopolysaccharides of the outer membrane layer and folding of some lipoproteins. Coupled with this study, these studies suggest that the stiffness of a dead cell depends not only on the cell type but on the method of cell death.

Hydrostatic Pressure-Induced Stress

Hydrostatic pressure is a classic physical stress, known to induce and maintain complex reactions in living cells. *In vivo* variations in hydrostatic pressure induced from body weight and normal activity

"Dead" chondroblast
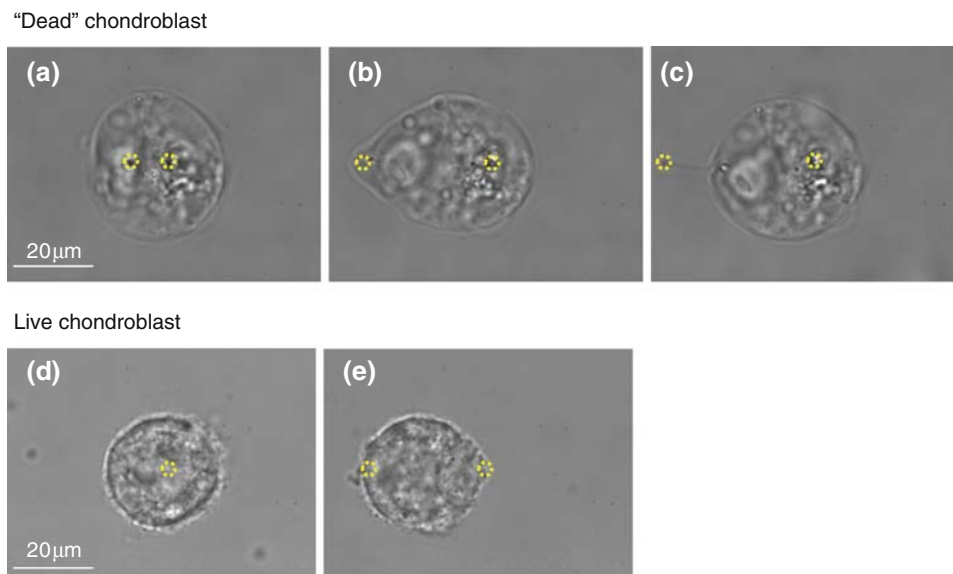

Live chondroblast

FIGURE 5. The deformation of chondroblasts by the relative movement of 2 optical traps. The dashed circles show the trap locations.

constantly act on bone and cartilage cells. These pressure variations are known to play an important role in mechanotransduction. *In vitro* studies performed on osteoblast cultures have shown that mechanical stimulation by hydrostatic compression plays a role in regulating osteoblast metabolism, promoting the synthesis of signaling molecules and other molecules pertinent to new bone formation.[15,17,58] Focusing on only the mechanical response, Wilkes and Athanasiou[73] have demonstrated that osteoblast-like cells, suspended in media, are incompressible under hydrostatic pressures to up to 7 MPa. Following conventional hydrostatic compression procedures, Smith *et al.*[64] and Parkkinen *et al.*[51] observed cellular and metabolic responses to increases in hydrostatic pressures up to 10 MPa. Parkkinen *et al.*[51] noticed a significant increase in the $^{35}SO_4$ uptake for a 0.5 MPa load during 50 ms repeated at 4-s intervals. Toyoda *et al.*[68] applied hydrostatic pressure at 5 MPa for a 4-h loading period to chondrocytes cultured in 3-dimensional agarose gels. They observed a change in proteoglycan metabolism but no cell deformation. However a cellular response was detected for pressures as low as 5.86 kPa where continuous hydrostatic pressure enhanced the calcium intake and inhibited the accumulation of cAMP in cartilage cells.[3]

In this study chondrocytes were trapped and hydrostatic pressure, P_{static}, varied. $P_{static} = \rho g h$, where ρ is the fluid density ($\rho = 10^3$ kg m^{-3}), g is gravity ($g = 9.81$ m s^{-2}), and h is the height difference (0–20 cm) between the input and output syringes. The laser power was set as low as possible, but sufficient to suspend a cell and position it in the microscope focal plane. For the limited range of hydrostatic pressures examined (0–2 kPa), no significant volume change was recorded due to a change in hydrostatic pressure. This is not surprising as the pressures applied are quite small when compared to other studies that show no deformation at significantly higher pressures. With the applied technique, the maximum pressure that can be applied to an optically suspended cell is limited by the structural integrity of the coverslip. The microfluidic interconnects, chip materials (other than the coverslip), and chip bonding methods can withstand pressure in excess of 1.5 MPa. A previous study examining coverslip strength reports coverslip failure at pressures of ~200 kPa.[53] At this maximum pressure (200 kPa) it is highly unlikely that a significant volume change would occur for an optically suspended cell. However, it is still unclear as to the extent small pressure perturbations up to 200 kPa can induce biological responses (Smith *et al.*[64] and Parkkinen *et al.*[51] observed a biological response at 500 kPa). Further experiments at higher pressures that monitor the biological response are necessary to explore this possibility.

Hydrodynamic-Induced Stress: Uniform Flow

A number of cell monolayer studies show that fluid flow is an influential mediator in bone remodeling and that the signaling response of osteoblasts depends on the flow profile. Reich *et al.*,[57] Johnson *et al.*,[25] Chen *et al.*[8] and Kapur *et al.*[30] have shown that osteoblasts respond to laminar flow shear stresses by changing their concentration of biochemical signals such as Nitric Oxide and intracellular [Ca^{2+}]. McAllister and Frangos[44] discovered that flow transients had greater effect on the stimulation of Nitric Oxide production. You *et al.*,[77] Donahue *et al.*[10] and Mullender *et al.*[47] observed that the biochemical response of osteoblasts increased during oscillating flows. This effect depends on both the flow amplitude (shear stress from 0.6 to 4 Pa) and frequency. Kwon and Jacobs[36] examined the morphological response of adhered osteoblasts to steady and oscillating flows. Their results suggest that viscous deformation occurs during steady flow, while elastic deformation develops during oscillatory flows of physiological frequency (~1 Hz).

The above studies demonstrate the importance of fluid flow on mechanotransduction. However, in these cell monolayers studies, cells are attached to a glass slide and frequently attached to neighboring cells. Therefore, the cells are mechanically constrained and stimulated unevenly throughout their body. With the μPIVOT, a single OT can hold a cell against an imposed fluid flow generated by the movement of the automated stage. Under these conditions, a cell is subjected to three dimensional stresses with no physical attachment. Two experimental parameters are examined here in response to this flow state, the cell deformation, and the trap stiffness.

Figure 6 shows (a) a chondroblast in a quiescent fluid, and (b) the same chondroblast subjected to a unidirectional flow of 50 μm/s fluid velocity. Figure 6b shows a clear shift of the cell to the right during flow conditions with the cell flattened slightly on the

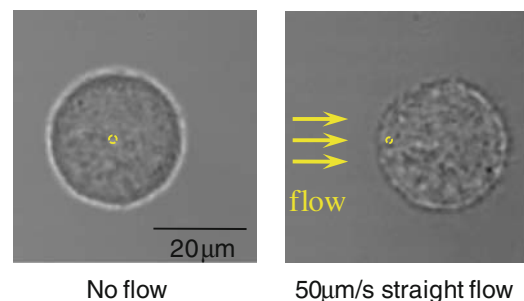No flow   50μm/s straight flow

FIGURE 6. A 19.1 μm diameter chondroblast in static suspension (left). Visible cellular deformation of the cell due to an applied fluid shear stress induced by a straight channel flow (right). The circle represents the trap size (approximately 1.6 μm in diameter) and location.

upstream face due to hydrodynamic pressure. The calculated cell deformation was $D_{12} = 0.03$. For the applied laser power (30 mW at the sample to avoid cell photodamage), the drag force can easily exceed the optical trap force. Therefore, the magnitude of induced fluid stresses is limited and larger cell deformation is not possible. For these experiments, the maximum applied flow velocity was 100 μm/s which, with a culture media viscosity of $\mu = 1$ mPa s, a cell radius, $a = 10$ μm, and the distance to the coverslip, $l = 30$ μm, corresponds to a maximum drag force of approximately 28 pN. Assuming the cell is a solid rigid sphere subjected to uniform creeping flow, the maximum shear (τ) and normal (σ) stresses are[33,38] $\tau_{max} = \sigma_{max} = 3\mu v_\infty/2a$, where μ is the fluid viscosity, a is the cell radius, and v_∞ is the fluid velocity. With the culture media viscosity equal to 1 mPa s and a cell radius of 10 μm, the maximum shear stress applied to the cell was approximately 15 mPa. While this fluid induced stress is roughly 60 times smaller than typical shear stresses applied uniformly along only the exposed cell surface during cell monolayer studies, the stress is varied across the entire cell surface. In this experiment the cell is indeed entirely exposed to the flow instead of having a large attached surface not experiencing any fluid stress.

As described earlier, trap stiffness is calculated by measuring the cell displacement from its equilibrium, no flow position. Trap stiffness is known to depend, among other parameters, on the properties of the object being trapped. Therefore, trap stiffness may be a source of information to characterize cellular properties. For example, cells could be the same type (for example chondroblasts) but have dissimilar actin filament distributions or orientations, intracellular fluid composition, etc., due to a difference in their location (e.g. different layers of cartilage) or healthy vs. diseased states. The differences in their intracellular constitution could affect the trap stiffness, and thus provide a means to identify influences on cell behavior. In this study, eleven chondroblasts extracted at different passages (P2, P3 and P4) and from different layers of cartilage were trapped in a straight flow and their corresponding trap stiffness calculated. The purpose of this study was to determine the reproducibility of the experiment and the potential range of linear trap stiffness values. Figure 7 shows the trap stiffness is confined within the range of 0.84 and 1.73 pN/μm (average = 1.20 pN/μm, standard deviation = 0.27 pN/μm). This wide range yields a potential 57% difference in trap stiffness between varying cells. Figure 8 shows a representative result for multiple trap stiffness measurements on the same cell. This P2, 16.5 μm diameter chondroblast was initially tested under an OT power of 30 mW then 130 mW for 3 min under an applied drag force. The cell
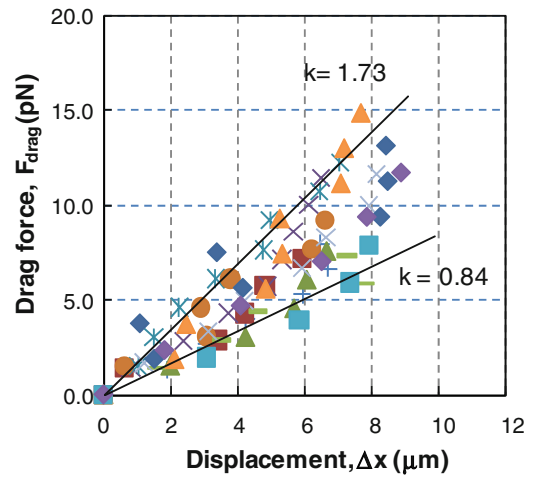

FIGURE 7. Cell displacement as a function of fluid drag for P2, P3 and P4 chondroblasts with 13.5–23 μm diameters. The trap stiffness (*k*) is determined from the slope of F_{drag} vs. Δx. The maximum variation in trap stiffness is 57%. The lines represent the maximum and minimum trap stiffness calculations.
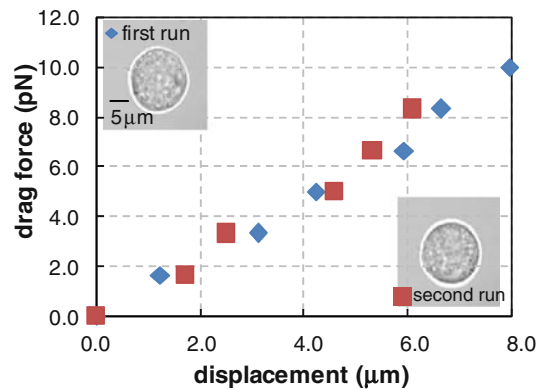

FIGURE 8. Drag force vs. displacement for a 16.5 μm diameter chondroblast (P2). The experiment was repeated with the same cell to assess the variability due to the measurement technique. The trap stiffness was measured to be approximately 1.2 pN/μm with a difference of 3.7% between the two runs.

was then re-tested at 30 mW. The total experiment time of was 15 min and no morphological change or reorientation of the cell was observed. The average trap stiffness was measured to be 1.2 pN/μm with a difference of 3.7% between the two runs. The variations in trap stiffness for all the cells studied in two consecutive runs under the same conditions was calculated to be between 0.9 and 8.6% (average = 3.7%, standard deviation = 3.5%), with a typical difference of 3–4% which is consistent with the 5% expected uncertainty in the drag force calculation. These results show a small trap stiffness variability and indicate that an individual cell may have a preferred trapped configuration. Thus,

the errors in the measurement technique are insufficient to generate the wide range observed in Fig. 7. This indicates that the variation in Fig. 7 is not due to the measurement technique, but due to the variations in cell properties (age, culture time, passage, morphology, size, etc.). This suggests the possibility to identify cell properties through trap stiffness measurements.

Hydrodynamic-Induced Stress: Extensional Flow

For uniform flows, the magnitude of fluid induced stresses is limited by the maximum optical trap forces that may be applied without optically damaging the cell. To apply stresses similar to cell monolayer studies, a laser power of ~1 W would be required. As described in the "Cell Viability During Optical Tweezing" section this would inflict cell damage within ~20 s and cell death after 35 s. Therefore, in order to apply similar fluid induced shear stresses on the cell without inflicting optical damage, flows in which fluid drag is negligible are required. As described earlier, a cross-junction flow geometry creates an extensional flow where the cell is compressed and stretched at the stagnation point. Theoretically, a cell centered at a stagnation point experiences no net drag force and remains there indefinitely regardless of the magnitude of shear/extensional rate. In practice, the stagnation point represents a saddle point, unstable to perturbations

in cell position. However, the cell may be maintained at that location by applying small restoring forces (with the OT) to counteract any perturbations. These restoring forces are substantially smaller than the drag force on a cell in a uniform flow with equivalent shear rates. Maintaining the cell at the stagnation point eliminates the drag force and thus minimizes the laser power required to apply higher fluid induced stresses. This reduces the possibility of deleterious heating and photodamage.

Figure 9a shows a polystyrene sphere (a model cell) suspended in a cross junction flow. The velocity field is measured with the μPIV function of the μPIVOT to characterize the local flow state. From these velocities, the local stresses applied to the suspended sphere may be calculated. Kohles et al.[33] calculated the fluid stresses for a rigid sphere suspended at the stagnation point of a planar extensional flow. Figure 9c depicts the theoretical normalized maximum shear and normal stresses occurring along the sphere surface. The maximum shear and normal stresses at the surface are

$$\tau_{max} = \sigma_{max} = 5\mu\gamma$$

Figure 9b shows the type and location of the maximum stresses applied to the sphere. The maximum shear stress, τ_{max}, occurs at an angle of $\theta = 45°$; the maximum compressive and tension stresses (σ_{max})
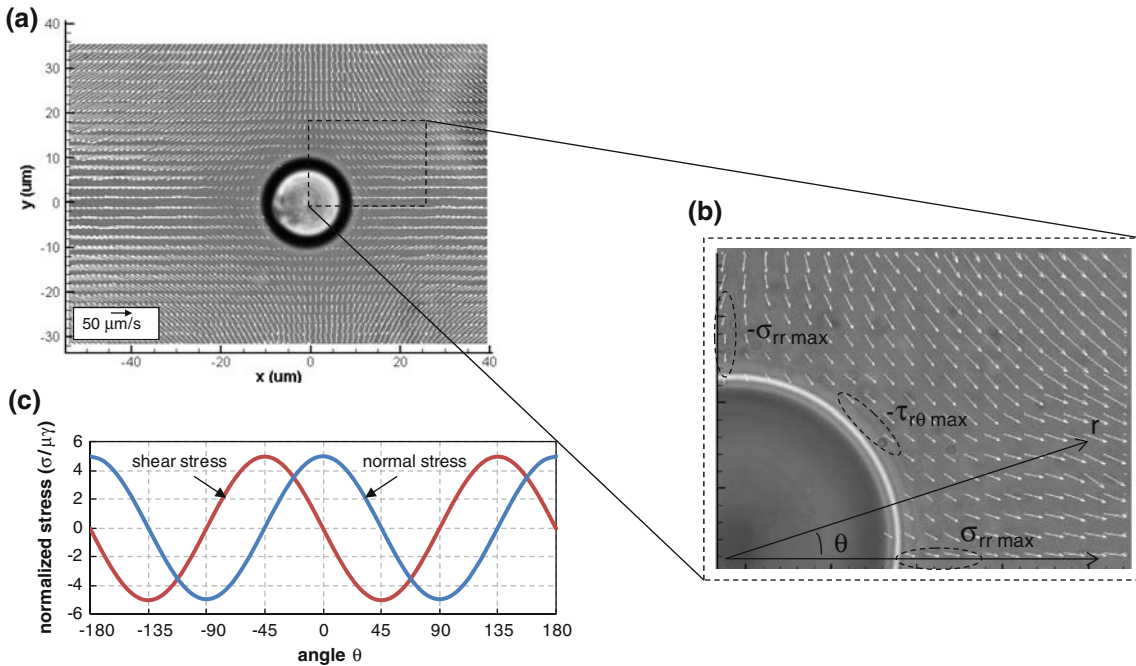

FIGURE 9. (a) The localized velocity field near a polystyrene sphere at the cross-flow region measured with μPIV. (b) Expanded view of the sphere quadrant and surrounding fluid with the location of the maximum shear, tension and compression stresses applied at the surface of the sphere. (c) The theoretical normalized shear, $\tau_{r\theta}$ (red line) and normal, σ_{rr} (blue) stresses at the surface of a sphere ($r = a$).
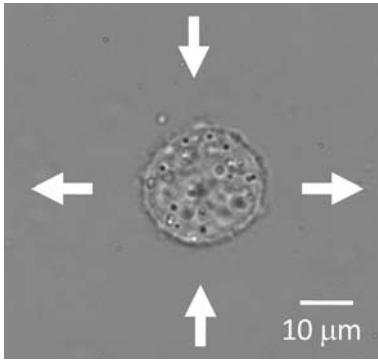
FIGURE 10. A living, 20 μm diameter osteoblastic optically trapped in the microfluidic cross-junction flow. The arrows are drawn to illustrate the flow direction.

FIGURE 11. Deformation characteristics of a myoblast subjected to the cross junction extensional flow. Low extension rate (<7.8 s^{-1}) and high extension rate (>7.8 s^{-1}) deformation regimes are observed.

occur for $\theta = 90°$ and $0°$, respectively. It is interesting to note that contrary to uniform flow, the maximum stress applied on the sphere doesn't depend on its size, but only on the fluid viscosity and the fluid strain rate. Additionally, with the drag force equal to zero at the stagnation point, the maximum possible shear stresses may exceed those possible during cell monolayer studies and are only limited by the geometry and flow rate of the microfluidic cross-junction chips as well as the ability to position and maintain the cell at the stagnation point.

Figure 10 shows a live osteoblastic cell (~20 μm in diameter) optically trapped in a microfluidic cross-junction flow. Video 1 shows the extensional flow going around the cell, 12.4 times slower than in real time. The image and video illustrate the capabilities of the μPIVOT to trap a cell and maintain its position at the stagnation point. For the experimental conditions of Fig. 10 ($\gamma = 10$ s^{-1}) and Video 1, no deformation of the osteoblastic cell was observed. With a culture media viscosity of ~1 mPa s and a current maximum undisturbed flow extension rate of 50 s^{-1} (current manual positioning of the cell at the stagnation point limits further increases) the maximum potential stress that may be applied to a cell in a cross junction is approximately 250 mPa. This is an order of magnitude higher than the maximum stresses achievable with uniform flow and a factor of ~4 smaller than cell monolayer studies. Automation of the trap positioning and active control of the cell position relative to the stagnation point should enable substantially greater shear stresses (in excess of 1 Pa). Such control schemes have been used successfully to examine drop deformation in planar extensional flows[4,69] over a large range of extension rates.

In contrast to the relatively stiff osteoblastic cell, Fig. 11 provides the deformation of a myoblast (C2C12 muscle cells) as a function of the fluid extension ra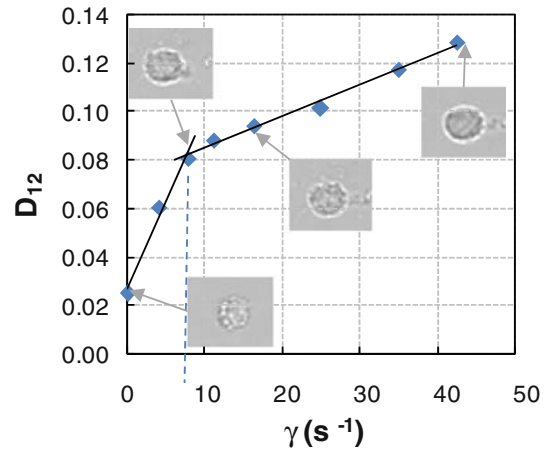te in the cross junction. Note that an initial asymmetry of the myoblast exists, $D_{12} = 0.027$ at $\gamma = 0$. At smaller extension rates, the cell deforms linearly with a slope of ~6.9×10^{-3} s. At higher extension rates, the deformation is linear was well, but with a slope of 1.5×10^{-3} s. The two linear regimes were identified by linearly fitting the data starting from either the lowest or highest data point respectively and calculating the R^2 value as each successive data point was added. The lines plotted represent a linear fit with $R^2 > 0.98$ that incorporated a maximum number of data points (3 points for the low regime and 6 points for the high regime). The results suggest a modulated response of the cell to the applied shear and normal stresses with a low extension rate regime below ~7.8 s^{-1} and a high extension rate regime above ~7.8 s^{-1}. From a drop deformation perspective, this behavior would be consistent with a non-Newtonian shear thickening material.

To the best of our knowledge, the above experiments represent the first time an osteoblast or myoblast has been optically suspended and manipulated in a extensional flow microenvironment (Hudson *et al.*[22] positioned a red blood cell in a low shear rate extensional flow environment by controlling the flow rates in opposite flow channels). This microfluidic manipulation and subsequent analysis may provide new insight on the response of cells to different mechanical stimuli. Moreover, the deformation results provided by these cell experiments could be directly compared to drop deformation analysis in extensional flows. Extensive drop deformation studies have been conducted with an emphasis on fluid type (Newtonian vs. non-Newtonian),[5,70] visco-elastic bodies,[11] and variations in interfacial properties.[69] Additionally, numerical and theoretical models incorporating these effects are

relatively abundant.[56] With this difference in perspective, a drop deformation comparison may provide insight into modeling cell mechanics and help characterize the viscoelastic properties of cells.

Comment on Relevance to Mechanotransduction

While single cell suspension is dissimilar from *in vivo* conditions, where bone and cartilage cells are living in a dynamic fluid and surface microenvironment, this technique may provide insight into the mechanotransduction process. Specifically, the mechanism associated with cell attachment is highly complex and not fully understood. By suspending a cell then incorporating controlled stresses and interactions including cell attachment, the effects of a specific interaction may be elucidated from other contributing factors. Additionally, with the imaging and velocity field characterization of μPIV, the actual morphology and stress state of a suspended cell can be accurately measured. Thus, the cell's mechanical response can be directly related to the applied stresses without model interpretation of results. To further address mechanotransduction, the cell biological response to mechanical stimulation must be characterized. Intracellular calcium concentration, as well as Nitric Oxide production are recognized to increase under certain types of mechanical loadings, and the actin cytoskeleton of the cell is known to vary with cell attachment.[67] Significant research in microfluidics focuses on chemical and biological detection techniques.[31,34,76] These techniques can be integrated with the μPIVOT to identify different molecule or ion concentrations and to analyze the biochemical response of the cell to mechanical stimuli.

SUMMARY

The μPIVOT is an instrument combining dual optical tweezers (OT) and micron resolution particle image velocimetry (μPIV). Combined with microfluidics, it is a novel tool to study single cell biomechanics. Cells may be subjected to three dimensional stress fields applied in sequence or simultaneously by stretching of the cell with the dual optical tweezers, compression through hydrostatic pressure, and shear, compression, and extension from uniform or extensional flows. The initial studies indicate (1) a dead cell deforms globally more than a viable cell and presents less resistance to internal organelle rearrangement, (2) at the typical laser power (30 mW at the sample) cell photodamage is negligible for at least 20 min while at maximum laser powers (~1 W at the sample) photodamage is observed after ~20 s with cell death

occurring after 35 s, (3) for uniform flows, the maximum fluid induced shear stresses are limited by cell damage to ~15 mPa which is 60 times less than cell monolayer studies, (4) for extensional flow in a microfluidic cross junction, shear stresses of 250 mPa were achieved and substantially greater shear stresses may be applied to suspended cells by automation of trap positioning and active control of the cell position relative to the stagnation point, and 5) while osteoblasts show no deformation in extensional flow for shear stresses up to 250 mPa, a myoblast is easily deformed in an extensional flow and exhibits a low extension rate and high extension rate deformation regime.

With the μPIVOT and microfluidics global and/or local stresses may be applied to a cell without physical contact allowing a new realm of tests to be performed *in vitro* at the single cell level. This realm of tests may provide novel information on the mechanical response of cells to mechanical stimuli. Coupled with chemical and biological sensors, the μPIVOT and microfluidics may bring us closer to understanding the biochemical responses of single cells to mechanical stimuli and the role of physical attachment in the mechanotransduction mechanism.

ELECTRONIC SUPPLEMENTARY MATERIAL

The online version of this article (doi:10.1007/s12195-010-0113-3) contains supplementary material, which is available to authorized users.

ACKNOWLEDGMENTS

REFERENCES

[1]Ashkin, A., and J. M. Dziedzic. Optical trapping and manipulation of viruses and bacteria. *Science* 235(4795): 1517–1520, 1987.
[2]Ashkin, A., J. M. Dziedzic, and T. Yamane. Optical trapping and manipulation of single cells using infrared-laser beams. *Nature*. 330(6150):769–771, 1987.

[3]Bourret, L. A., and G. A. Rodan. The role of calcium in the inhibition of cAMP accumulation in epiphyseal cartilage cells exposed to physiological pressure. *J. Cell Physiol.* 88(3):353–362, 1976.

[4]Bentley, B. J., and L. G. Leal. A computer-controlled four-roll mill for investigations of particle and drop dynamics in two-dimensional linear shear flows. *J. Fluid Mech.* 167:219–240, 1986.

[5]Bentley, B. J., and L. G. Leal. An experimental investigation of drop deformation and break-up in steady, two-dimensional flows. *J. Fluid Mech.* 167:241–283, 1986.

[6]Bull, B., C. Feo, and M. Bessis. Behavior of elliptocytes under shear stress in the rheoscope and ektactometer. *Cytometry* 3(4):300–304, 1983.

[7]Cerf, A., J. C. Cau, C. Vieu, and E. Dague. Nanomechanical properties of dead or alive single-patterned bacteria. *Langmuir* 25(10):5731–5736, 2009.

[8]Chen, N. X., K. D. Ryder, F. M. Pavalko, C. H. Turner, D. B. Burr, J. Qiu, and R. L. Duncan. Ca^{2+} regulates fluid shear-induced cytoskeletal reorganization and gene expression in osteoblasts. *Am. J. Physiol. Cell Physiol.* 278:C989–C997, 2000.

[9]Declercq, H., N. Van den Vreken, E. De Maeyer, R. Verbeeck, E. Schacht, L. De Ridder, and M. Cornelissen. Isolation, proliferation and differentiation of osteoblastic cells to study cell/biomaterial interactions: comparison of different isolation techniques and source. *Biomaterials* 25:757–768, 2004.

[10]Donahue, T. L., T. R. Haut, C. E. Yellowley, H. J. Donahue, and C. R. Jacobs. Mechanosensitivity of bone cells to oscillating fluid flow induced shear stress may be modulated by chemotransport. *J. Biomech.* 36:1363–1371, 2003.

[11]Eggleton, C. D., Y. P. Pawar, and K. J. Stebe. Insoluble surfactants on a drop in an extensional flow: a generalization of the stagnated surface limit to deforming interfaces. *J. Fluid Mech.* 385:79–99, 1999.

[12]Evans, E., and A. Yeung. Apparent viscosity and cortical tension of blood granulocytes determined by micropipet aspiration. *Biophys. J.* 56(1):151–160, 1989.

[13]Fallman, E., and O. Axner. Influence of a glass–water interface on the on-axis trapping of micrometer-sized spherical objects by optical tweezers. *Appl. Opt.* 42:3915, 2003.

[14]Felder, S., and E. L. Elson. Mechanics of fibroblast locomotion: quantitative analysis of forces and motions at the leading lamellas of fibroblasts. *J. Cell Biol.* 111:2513–2526, 1990.

[15]Ferraro, J. T., M. Daneshmand, R. Bizios, and V. Rizzo. Depletion of plasma membrane cholesterol dampens hydrostatic pressure and shear stress-induced mechanotransduction pathways in osteoblast cultures. *Am. J. Physiol. Cell Physiol.* 286:C831–C839, 2004.

[16]Francius, G., O. Domenech, M. P. Mingeot-Leclercq, and Y. F. J. Dufrene. Direct observation of Staphylococcus aureus cell wall digestion by Lysostaphin. *J. Bacteriol.* 190(24):7904–7909, 2008.

[17]Glantschnig, H., F. Varga, and M. Rumpler. Prostacyclin (PGI2): a potential mediator of c-fos expression induced by hydrostatic pressure in osteoblastic cells. *Eur. J. Clin. Invest.* 26:533–548, 1996.

[18]Guck, J., R. Ananthakrishnan, H. Mahmood, T. J. Moon, C. C. Cunningham, and J. Käs. The optical stretcher: a novel laser tool to micromanipulate cells. *Biophys. J.* 81(2):767–784, 2001.

[19]Happel, J., and H. Brenner. Low Reynolds Number Hydrodynamics (2nd ed.). Dordecht, the Netherlands: Kluwer Academic, p. 553, 1991.

[20]Hassan, E., W. F. Heinz, M. D. Antonik, N. P. D'Costa, S. Nageswaran, C. A. Schoenenberger, and J. H. Hoh. Relative microelastic mapping of living cells by atomic force microscopy. *Biophys. J.* 74:1564–1578, 1998.

[21]Hochmuth, R. M., and R. E. Waugh. Erythrocyte membrane elasticity and viscosity. *Annu. Rev. Physiol.* 49:209–219, 1987.

[22]Hudson, S. D., F. R. Phelan, M. D. Handler, J. T. Cabral, K. B. Migler, and E. J. Amis. Microfluidic analog of the four-roll mill. *Appl. Phys. Lett.* 85(2):335–337, 2004.

[23]Im, K. B., H. I. Kim, I. J. Joo, C. H. Oh, S. H. Song, P. S. Kim, and B. C. Park. Optical trapping forces by a focused beam through two media with different refractive indices. *Opt. Commun.* 226:25–31, 2003.

[24]Jaasma, M., W. Jackson, R. Tang, and T. Keaveny. Adaptation of cellular mechanical behavior to mechanical loading for osteoblastic cells. *J. Biomech.* 40(9):1938–1945, 2007.

[25]Johnson, D. L., T. N. McAllister, and J. A. Frangos. Fluid flow stimulates rapid and continuous release of nitric oxide in osteoblasts. *Am. J. Physiol. Endocrinol. Metab.* 271:E205–E208, 1996.

[26]Jones, G. E. Human Cell Culture Protocols. Totowa, NJ: Humana Press, 1996.

[27]Jones, W. R., H. P. Ting-Beall, G. M. Lee, S. S. Kelley, R. M. Hochmuth, and F. Guilak. Alterations in the Young's modulus and volumetric properties of chondrocytes isolated from normal and osteoarthritic human cartilage. *J. Biomech.* 32(2):119–127, 1999.

[28]Kamm, R. D., and M. R. Kaazempur-Mofrad. On the molecular basis for mechanotransduction. *Mech. Chem. Biosystems* 1(3):201–209, 2004.

[29]Kaneta, T., J. Makihara, and T. Imasaka. An "optical channel": a technique for the evaluation of biological cell elasticity. *Anal. Chem.* 73(24):5791–5795, 2001.

[30]Kapur, S., D. J. Baylink, and K. H. W. Lau. Fluid flow shear stress stimulates human osteoblast proliferation and differentiation through multiple interacting and competing signal transduction pathways. *Bone* 32(3):241–251, 2003.

[31]Kim, J., M. Junkin, D. H. Kim, S. Kwon, Y. S. Shin, P. K. Wong, and B. K. Gale. Applications, techniques, and microfluidic interfacing for nanoscale biosensing. *Microfluid. Nanofluid.* 7:149–167, 2009.

[32]Koay, E. J., A. C. Shieh, and K. A. Athanasiou. Creep indentation of single cells. *J. Biomech. Eng.* 125(3):334–341, 2003.

[33]Kohles, S. S., N. Nève, J. D. Zimmerman, and D. C. Tretheway. Mechanical stress analysis of microfluidic environments designed for isolated biological cell investigations. *ASME J. Biomech. Eng.* 131:121006(10 pages), 2009.

[34]Kraly, J. R., R. E. Holcomb, Q. Guan, and C. S. Henry. Review: microfluidics applications in metabolomics and metabolic profiling. *Anal. Chem. Acta* 653:23–35, 2009.

[35]Kuo, S. C., and M. P. Sheetz. Optical tweezers in cell biology. *Trends Cell Biol.* 2:116–118, 1992.

[36]Kwon, R. Y., and C. R. Jacobs. Time-dependent deformations in bone cells exposed to fluid flow in vitro: investigating the role of cellular deformation in fluid flow-induced signaling. *J. Biomech.* 40(14):3162–3168, 2007.

[37]Lang, M., C. Asbury, J. Shaevitz, and S. M. Block. An automated two-dimensional optical force clamp for single molecule studies. *Biophys. J.* 83:491–501, 2002.

[38]Leal, L. G. Laminar Flow and Convective Transport Processes: Scaling Principles and Asymptotic Analysis. Boston, MA: Butterworth-Heinemann, 1992.

[39]Leipzig, N. D., and K. A. Athanasiou. Unconfined creep compression of chondrocytes. *J. Biomech.* 38:77–85, 2005.

[40]Liang, H., K. T. Vu, P. Krishnan, T. C. Trang, D. Shin, S. Kimel, and M. W. Berns. Wavelength dependence of cell cloning efficiency after optical trapping. *Biophys. J.* 70:1529–1533, 1996.

[41]Liao, G.-B., P. B. Bareil, Y. Sheng, and A. Chiou. One-dimensional jumping optical tweezers for optical stretching of bi-concave human red blood cells. *Opt. Express* 16(3):1996–2004, 2008.

[42]Liu, Y., D. Cheng, G. J. Sonek, M. W. Berns, C. F. Chapman, and B. J. Tromberg. Evidence for localized cell heating induced by infrared optical tweezers. *Biophys. J.* 68:2137–2144, 1995.

[43]Liu, Y., G. J. Sonek, M. W. Berns, and B. J. Tromberg. Physiological monitoring of optically trapped cells: assessing the effects of confinement by 1064-nm laser tweezers using microfluorometry. *Biophys. J.* 71:2158, 1996.

[44]McAllister, T. N., and J. A. Frangos. Steady and transient fluid shear stress stimulate NO release in osteoblasts through distinct biochemical pathways. *J. Bone Miner. Res.* 14:930–936, 1999.

[45]Meinhart, C. D., S. Wereley, and J. Santiago. A PIV algorithm for estimating time-averaged velocity fields. *J. Fluid. Eng.* 122:285, 2000.

[46]Mills, J. P., L. Qie, M. Dao, C. T. Lim, and S. Suresh. Nonlinear elastic and viscoelastic deformation of the human red blood cell with optical tweezers. *MCB* 1(3):169–180, 2004.

[47]Mullender, M. G., S. J. Dijcks, R. G. Bacabac, C. M. Semeins, J. J. W. A. Van Loon, and J. Klein-Nulend. Release of nitric oxide, but not prostaglandin E2, by bone cells depends on fluid flow frequency. *J. Orthop. Res.* 24(6):1170–1177, 2006.

[48]Neuman, K. C., E. H. Chadd, G. F. Liou, K. Bergman, and S. M. Block. Characterization of photodamage to *Escherichia coli* in optical traps. *Biophys. J.* 77(5):2856, 1999.

[49]Nève, N., J. K. Lingwood, J. Zimmerman, S. S. Kohles, and D. C. Tretheway. The μPIVOT: an integrated particle image velocimeter and optical tweezers instrument for microenvironment investigations. *Meas. Sci. Technol.* 10(9):095403(11 pp.), 2008.

[50]Nguyen, M., and S. Wereley. Fundamentals and Applications of Microfluidics. Norwood, MA: Artech Hous Publishers, 2002.

[51]Parkkinen, J. J., J. Ikonen, M. J. Laman, J. Laakonen, M. Tammi, and H. J. Helminen. Effects of cyclic hydrostatic pressure on proteoglycan synthesis in cultured chondrocytes and articular cartilage explants. *Arch. Biochem. Biophys.* 300:458–465, 1993.

[52]Pasternak, C., and E. L. Elson. Lymphocyte mechanical response triggered by cross-linking surface receptors. *J. Cell Biol.* 100:860–872, 1985.

[53]Peake, M. A., L. M. Cooling, J. L. Magnay, P. B. M. Thomas, and A. J. El Haj. Selected contribution: regulatory pathways involved in mechanical induction of c-fos gene expression in bone cells. *J. Appl. Physiol.* 89(6):2498–2507, 2000.

[54]Petersen, N. O., W. B. McConnaughey, and E. L. Elson. Dependence of locally measured cellular deformability on position on the cell, temperature, and cytochalasin b. *Proc. Natl Acad. Sci. USA* 79:5327–5331, 1982.

[55]Radmacher, M. Measuring the elastic properties of living cells by the atomic force microscope. *Methods Cell Biol.* 68:67–90, 2002.

[56]Ramaswamy, S., and L. G. Leal. The deformation of a viscoelastic drop subjected to steady uniaxial extensional flow of a newtonian fluid. *J. Non-Newtonian Fluid Mech.* 85:127, 1999.

[57]Reich, K. M., C. V. Gay, and J. A. Frangos. Fluid shear stress as a mediator of osteoblast cyclic adenosine monophosphate production. *J. Cell. Physiol.* 143:100–104, 1990.

[58]Roelofsen, J., J. Klein-Nulend, and E. H. Burger. Mechanical stimulation by intermittent hydrostatic compression promotes bone-specific gene expression in vitro. *J. Biomech.* 28:1493–1503, 1995.

[59]Rotsch, C., and M. Radmacher. Drug-induced changes of cytoskeletal structure and mechanics in fibroblasts—an atomic force microscopy study. *Biophys. J.* 78:520–535, 2000.

[60]Sato, M., M. J. Levesque, and R. M. Nerem. An application of the micropipette technique to the measurement of the mechanical properties of cultured bovine aortic endothelial cells. *J. Biomech. Eng.* 109:27–34, 1987.

[61]Schmid-Schönbein, G. W., K. L. Sung, H. Tözeren, R. Skalak, and S. Chien. Passive mechanical properties of human leukocytes. *Biophys. J.* 36(1):243–256, 1981.

[62]Schmid-Schönbein, H., R. Wells, and J. Goldstone. Influence of deformability of human red cells upon blood viscosity. *Circ. Res.* 25:131–143, 1969.

[63]Sleep, J., D. Wilson, R. Simmons, and W. Gratzer. Elasticity of the red cell membrane and its relation to hemolytic disorders: an optical tweezers study. *Biophys. J.* 77:3085–3095, 1999.

[64]Smith, L. R., S. F. Rusk, S. F. Ellison, P. Wessells, K. Tsuchiya, D. R. Carter, W. E. Caler, L. I. Sandel, and D. J. Schurman. In vitro stimulation of articular chondrocyte mRNA and extracellular matrix synthesis by hydrostatic pressure. *J. Orthop. Res.* 14:53–60, 1996.

[65]Sunk, I. G., S. Trattnig, W. B. Graninger, L. Amoyo, B. Tuerk, C. W. Steiner, J. S. Smolen, and K. Bobacz. Impairment of chondrocyte biosynthetic activity by exposure to 3-tesla high-field magnetic resonance imaging is temporary. *Arthritis Res. Ther.* 8(4):R106, 2006.

[66]Thoumine, O., A. Ott, O. Cardoso, and J.-J. Meister. Microplates: a new tool for manipulation and mechanical perturbation of individual cells. *J. Biochem. Biophys. Methods* 39:47–62, 1999.

[67]Titushkin, I., and M. Cho. Distinct membrane mechanical properties of human mesenchymal stem cells determined using laser optical tweezers. *Biophys. J.* 90:2582–2591, 2006.

[68]Toyoda, T., B. B. Seedhom, J. Q. Yao, J. Kirkham, S. Brookes, and W. A. Bonass. Hydrostatic pressure modulates proteoglycan metabolism in chondrocytes seeded in agarose. *Arthritis Rheum.* 48(10):2865–2872, 2003.

[69]Tretheway, D. C., and L. G. Leal. Surfactant and viscoelastic effects on drop deformation in 2-D extensional flow. *AIChE J.* 45(5):929–937, 1999.

[70]Tretheway, D. C., and L. G. Leal. Deformation and relaxation of Newtonian drops in planar extensional flows of a Boger Fluid. *J. Non-Newtonian Fluid Mech.* 99:81–108, 2001.

[71]Tretheway, D. C., and C. D. Meinhart. Apparent fluid slip at hydrophobic microchannel walls. *Phys. Fluids* 14:L9–L12, 2002.

[72]Wei, M.-T., A. Zaorski, H. C. Yalcin, J. Wang, M. Hallow, S. N. Ghadiali, A. Chiou, and H. D. Ou-Yang. A comparative study of living cell micromechanical properties by oscillatory optical tweezers. *Opt. Express* 16:8594–8603, 2008.

[73]Wilkes, R. P., and K. A. Athanasiou. The intrinsic incompressibility of osteoblast-like cells. *Tissue Eng.* 2(3): 167–181, 1996.

[74]Wu, L., M. Tsutahara, L. Kim, and M. Ha. Numerical simulations of droplet formation in a cross-junction microchannel by the lattice Boltzmann method. *Int. J. Numer. Meth. Fluids.* 57:793–810, 2008.

[75]Yang, C. H., K. S. Huang, P. W. Lin, and Y. C. Lin. Using a cross-flow microfluidic chip and external crosslinking reaction for monodisperse TPP-chitosan microparticles. *Sens. Actuators B Chem.* 124(2):510–516, 2007.

[76]Yi, C. Q., C. W. Li, S. L. Ji, and M. S. Yang. Microfluidics technology for manipulation and analysis of biological cells. *Anal. Chim. Acta* 560:1–23, 2006.

[77]You, J., G. C. Reilly, X. Zhen, C. E. Yellowley, Q. Chen, H. J. Donahue, and C. R. Jacobs. Osteopontin gene regulation by oscillatory fluid flow via intracellular calcium mobilization and activation of mitogen-activated protein kinase in MC3T3-E1 osteoblasts. *J. Biol. Chem.* 276:13365–13371, 2001.